# *In-situ Photogenerated Radicals of Hydroxyl Substitued Pyrene-based Triphenylamines with Enhanced Transport and Free Doping/Post-oxidation for Efficient Perovskite Solar Cells*

*Xiaohui Wang, Zhixin Xie, Rongxin Wang, Ye Xiao, Kai Yan, Yu Zhao, Rui Lin*, Carl Redshaw, Yonggang Min, Xinhua Ouyang*, and Xing Feng**

X. Wang., X. Xin, Dr. Y. Xiao, Prof. Y. Zhao, Prof. Y. Min, Prof. X. Feng
Guangdong Provincial Key Laboratory of Functional Soft Condensed Matter, School of Material and Energy, Guangdong University of Technology, Guangzhou 510006, P. R. China.
E-mail: hyxhn@sina.com (X. Feng)

R. Wang, Dr. R. Lin, Prof. X. Ouyang
Fujian Agriculture and Forestry University Fuzhou 350002, P. R. China.
E-mail: ouyangxh@fafu.edu.cn (X. Ouyang.), rui.lin@fafu.edu.cn (R. Lin)

K. Yan
Analysis and Test Center, Guangdong University of Technology, Guangzhou 510006, P. R. China.

C. Redshaw
Chemistry, School of Natural Sciences, University of Hull, Hull, Yorkshire HU6 7RX, UK.

Keywords: pyrene, hole transporting material, perovskite solar cells, power conversion efficiency, radical

The high-performance hole transporting material (HTM) is one of the most important components for the perovskite solar cells (PSCs) in promoting power conversion efficiency (PCE). However, the low conductivity of HTMs and their additional requirements for doping and post-oxidation greatly limits the device performance. In this work, three novel pyrene-based derivatives containing methoxy-substituted triphenylamines units (**PyTPA**, **PyTPA-OH** and

**PyTPA-2OH**) are designed and synthesized, where different numbers of hydroxyl groups are connected at the 2- or 2,7- positions of the pyrene core. These hydroxyl groups at the 2- or 2,7-positions of pyrene play a significantly role to enhance the intermolecular interactions which are able to generate *in situ* radicals with the assistance of visible light irradiation, resulting in enhanced hole transferring ability, as well as an enhanced conductivity and suppressed recombination. These pyrene-core based HTMs exhibit excellent performance in PSCs, which possess a higher PCE than those control devices using the traditional spiro-OMeTAD as the HTM. The best performance can be found in the devices with **PyTPA-2OH**. It has an average PCE of 23.44% ($PCE_{max}$ = 23.50%), which is the highest PCE among the reported PSCs with the pyrene-core based HTMs up to date. This research offers a novel avenue to design a dopant-free HTM by the combination of the pyrene core, methoxy triphenylamines and hydroxy groups.

## 1. Introduction

The perovskite solar cell (PSC) is the fastest developing photovoltaic technology, which shows great merits in lightweight, low-cost and good solution processability.[1] Over the past decades, tremendous efforts have been devoted into the optimization of perovskite recipes, interlayer materials and device configuration.[2] As a result, the power conversion efficiency (PCE) is dramatically enhanced from 3.80% to over 26.81 %,[3] which is approaching the numbers for commercialization.

The hole transporting material (HTM) plays an important role in the hole extraction. It helps to maintain the energy level alignment and passivates the interfacial defects, which directly determines the performance of the PSCs.[4] In 2012, Park *et al*. first demonstrated an all-solid-state PSC by replacing the liquid electrolytes with 2,2',7,7'-tetrakis(*N*,*N*-di-*p*-methoxy-phenylamine)-9,9'-spirobifluorene (spiro-OMeTAD) as the HTM. A PCE value of over 9% was achieved, which was among the state-of-the-art PSCs at that time. Up to now, the spiro-OMeTAD remains the dominant HTM for highly efficient PSCs, which has achieved a PCE of over 26%.[3d,5] However, pristine spiro-OMeTAD shows an undesirable hole mobility.[6] Additional doping and post-oxidation processes are required to increase the conductivity by creating radical cations.[7] Both oxygen and moisture will be introduced into the PSC during this post-oxidation process,[8] which seriously hampers both the reproducibility and stability of the PSCs.[9] Therefore, designing a dopant-free HTM without post-oxidation is crucial for the large-scale application of PSCs.

To achieve high performance, a dopant-free HTM should possess an excellent hole transfer ability, which requires a strong intermolecular interaction for π-π stacking.[10] Replacing the spirobifluorene core with π-conjugated fused rings is one of the effective strategies.[11] Martín *et al*.[12] reported a HTM using benzotrithiophene as the central core. Its planarized star-shaped molecular geometry leads to an effective π-π intermolecular interaction, which dramatically enhances the ability for hole transportation. Multiple HTMs with fused ring cores have been investigated for efficient hole transfer.[13] Recently, Wang *et al*.[14] utilized a large coplanar tetrathienopyrrole moiety as the core unit, which reinforces the molecular stacking and increases the hole mobility. Therefore, a coplanar π-conjugated central core is beneficial for the hole transportation in HTMs.[15]

Pyrene is a chemical by-product of the destructive distillation of coal tar, which is regarded as a classical building block for high-performance HTMs, due to its good thermal stability, large planar π-surface, rigid structure and high carrier mobility.[16] Many efficient pyrene-core based HTMs have been reported.[17] Seok *et al*.[18] first replaced the spirobifluorene core of spiro-OMeTAD with a pyrene core in 2013, which achieved comparable performance to spiro-OMeTAD. Later, Shao *et al*.[19] designed a two-dimensional molecule by further expanding this molecule using four phenyl-thiophene bridges. It exhibited a much higher hole mobility than that of spiro-OMeTAD, due to the effective delocalization and the enhanced intermolecular stacking. These results demonstrate the great potential of the pyrene core in achieving highly efficient HTMs for PSCs.

Increasing the radical density is another effective strategy to improve the performance of HTMs.[20] Triphenylamine (TPA) is a strong electron-donating unit, which exhibits the ability to form radicals due to its easily oxidizable nitrogen atom. Therefore, it has been widely applied as the main functional unit in HTMs.[21] Without *p*-doping and post-oxidation, TPA can only form radicals under UV irradiation.[22] However, UV exposure should be avoided during the operation of PSCs. The introduction of hydroxyl groups into the molecule may promote the formation of radicals. This may be attributed to the intramolecular electron transfer between the nitrogen atom and the hydroxyl group inside the molecule.[23] Alternatively, it could arise via intermolecular proton transfer from the hydroxyl group to the neighbouring nitrogen atom in a hydrogen-bonded dimeric structure.[24] Previously, our group presented new pyrene-based intermediates containing hydroxyl groups. The introduction of hydroxyl groups not only strengthens the intra/intermolecular interaction, but also plays a significant role in regulating the energy levels.[25] Inspired by these new pyrene-based intermediates, an efficient dopant-free HTM may be constructed through the combination of a pyrene core, TPAs and hydroxyl groups.

In this work, three novel HTMs (**PyTPA**, **PyTPA-OH** and **PyTPA-2OH**) are designed and synthesized using chemical-waste pyrene as the starting material. As displayed in **Scheme 1**, these molecules have a star-shaped structure with a pyrene core and four methoxy TPA arms.

Different numbers of hydroxyl groups are connected at the 2- and 7- positions of the pyrene core. All of these HTMs possess proper energy levels, which present good ability to achieve energy level alignment. Compared with the amorphous spior-OMeTAD,[26] these pyrene-core based molecules exhibit much higher crystallinity. The strong intermolecular interactions and the introduction of hydroxyl groups allows **PyTPA-OH** and **PyTPA-2OH** to create radicals with upon light irradiation. Both **PyTPA-OH** and **PyTPA-2OH** present a higher conductivity than the control spior-OMeTAD, which makes them excellent dopant-free HTMs for PSCs. The PSCs using **PyTPA-OH** and **PyTPA-2OH** as HTMs turn out to have a much better performance than the control devices (spiro-OMeTAD, 20.92%) with an average PCE of 22.46% and 23.44%, respectively. The best performance with a PCE of 23.50% is achieved in the PSC using **PyTPA-2OH**. It is the highest PCE value among the PSCs with the pyrene-core based HTMs up to date.

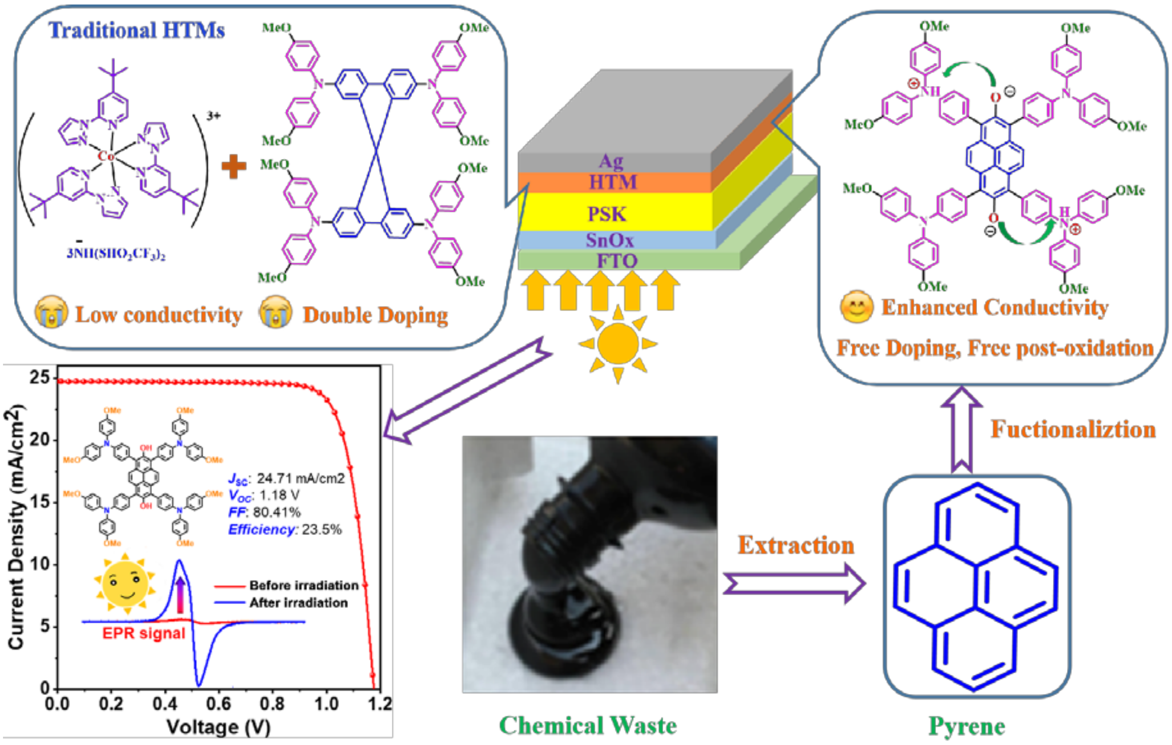

**Scheme 1**. Schematic from the traditional HTM to this work with improved properties.

## 2. Results

### 2.1. Molecular synthesis and thermal behavior

The molecular structures of **PyTPA**,[26] **PyTPA-OH**, **PyTPA-2OH**, and the control compound spiro-OMeTAD are shown in **Figure 1**; their synthetic routes are illustrated in **Scheme S1**. The Suzuki-Miyaura coupling reaction between (4-(bis(4-methoxyphenyl)amino)phenyl) boronic acid and the corresponding bromopyrene intermediates ensures the high yield of these target compounds. The final products were fully characterized by $^1H/^{13}C$ NMR spectroscopy and high-resolution mass spectrometry (HRMS), as shown in **Figures S1-S8**. All these materials start to decompose at a temperature above 440°C, confirming their excellent thermal stability. According to the differential scanning calorimetry results, **PyTPA**, **PyTPA-OH** and **PyTPA-2OH** display a relatively high crystallization temperature (>340°C) for the molecular packing rearrangement (**Figures S9-S12**). This indicates a stable crystalline structure of these HTMs, which may be attributed to their strong intermolecular interactions.

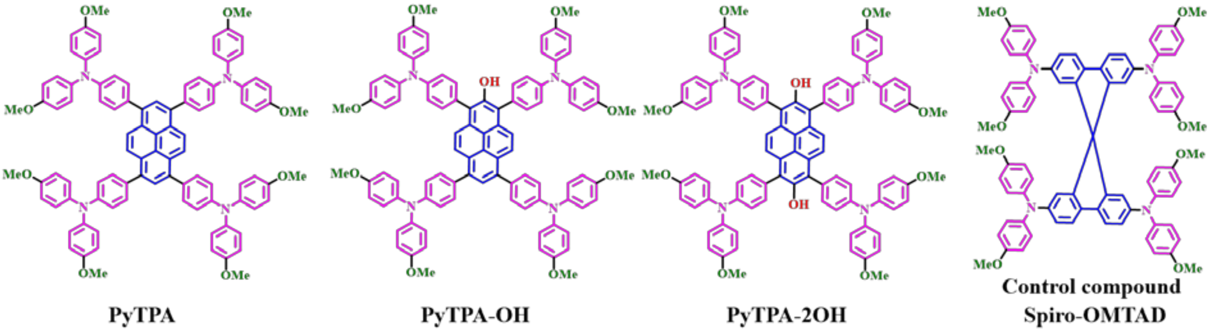

**Figure 1**. The structures of **PyTPA**, **PyTPA-OH**, **PyTPA-2OH**, and the control compound Spiro-OMeTAD.

## 2.2 X-ray diffraction analysis

The influence of the hydroxyl groups on the molecular structure and the intermolecular stacking were investigated through single crystal X-ray diffraction and powder X-ray diffraction, which are displayed in **Figure 2 and Figure S14** and **Table S1**. The crystals of **PyTPA**, **PyTPA-OH** and **PyTPA-2OH** were obtained via slow evaporation from a mixture of $CH_2Cl_2$ and hexane solution. **PyTPA** and **PyTPA-2OH** crystallize in a triclinic structure (P-1 space group). While, the **PyTPA-OH** crystal is found to be in the monoclinic system with $P\ 2_1/n$ space group. The four methoxy TPA arms are located at the 1-, 3-, 6-, and 8-positions of the pyrene core, which forms a twisted propeller-type conformation. The torsion angles between the methoxy-decorated TPA units and the pyrene core are in the range 40.1-57.4° for **PyTPA**. Connecting hydroxyl group(s) at the 2- or 2,7-positions of the pyrene core creates a steric effect. It increases this torsion angle to 54.1-60.5° in the case of **PyTPA-OH** and to 62.8-87.7° in the case of **PyTPA-2OH**. The enlarged torsion angle leads to a reduced crystal density. The crystal density of **PyTPA** is 1.372 mg $m^{-3}$. It gradually reduces to 1.275 Mg $m^{-3}$ for **PyTPA-OH** and to 1.234 mg $m^{-3}$ for **PyTPA-2OH**. In the **PyTPA-2OH** molecule, the C-O bond lengths between the pyrene core and hydroxy groups are 1.381 Å for the C15-O14 bond and 1.390 Å for the C21-O4 bond. The length of the C-O bond (C28-O3) in the **PyTPA-OH** crystal is 1.389 Å. These bonds are all shorter than regular C-O single bonds (~1.430 Å).[28] It suggests that the π-orbital of the oxygen atom conjugates with the *p*-orbital of the carbon atom, which tends to form a C=O like double bond and promotes the formation of radicals.[24]

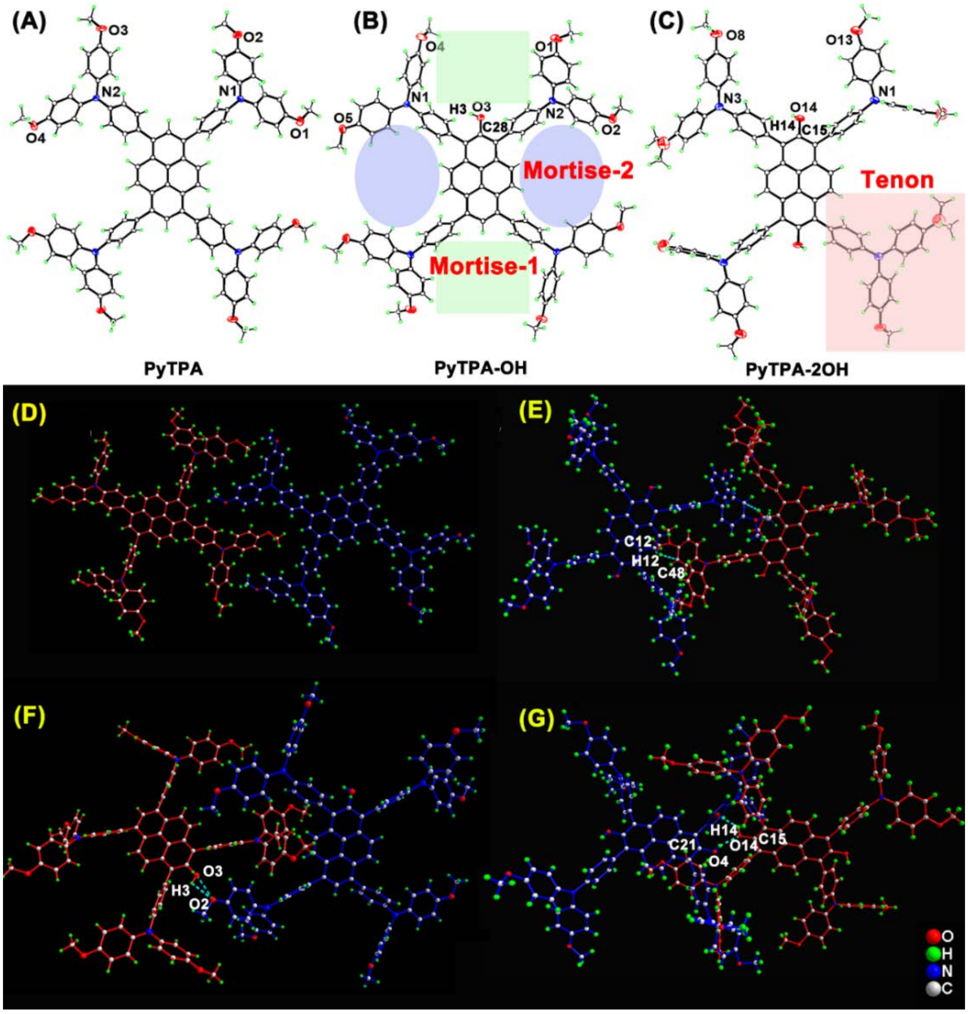

**Figure 2.** The single-crystal structures of (A) **PyTPA**; (B) **PyTPA-OH** and (C) **PyTPA-2OH** in an ORTEP drawing with thermal ellipsoids at 30% probability. Molecular packing of (D) **PyTPA**; (E) **PyTPA-2OH** and (F) **PyTPA-OH** along the *a*-axis. (G) Molecular packing of **PyTPA-2OH** along the *b*-axis.

All these molecules show a tenon and mortise like intermolecular stacking structure. As displayed in **Figure 2B**, the space between the methoxy TPA moieties can be treated as the mortise. The mortise-1 (marked as a green region) is the space between the methoxy TPAs at the 1- and 3-positions (or 6- and 8- positions) of the pyrene core. The mortise-2 (marked as blue region) is the space between the methoxy TPAs at the 1- and 8-positions (or 3- and 6-positions). The tenons are the methoxy TPAs at the 1-, 3-, 6- and 8- positions of the pyrene core (marked as a red region in **Figure 2C**). As shown in **Figures 2D** and **2E**, the methoxy TPA tenons will insert into the mortise-2 regions of the adjacent molecules. This forms an interlocked packing pattern along the *a*-axis, which is anchored by C-H···π interactions. As a consequence, **PyTPA** displays a ladder-type stacking conformation. Due to the presence of hydroxyl groups, another two kinds of packing geometries are detected. The hydroxyl group in the mortise-1 connects with the methoxyphenyl group from the methoxy TPA unit of the neighbouring molecule through a hydrogen bond (**Figure 2F**). The distance of this hydrogen bond in **PyTPA-OH** (O3-H3···O2) is 2.503 Å. The **PyTPA-2OH** molecule possesses two hydroxyl groups at the 2,7-positions of the pyrene core. It allows for an inter-crossed topological packing geometry through the connection of hydroxyl groups with a hydrogen bond (O4-H4···O14, 2.032 Å) between the adjacent molecules (**Figure 2G**). Meanwhile, the hydrogen atom (H14) of this hydroxyl group (-O14-H14) is in contact with the adjacent phenyl ring of the methoxy TPA unit via an O14-H14···π interaction (2.373 Å). It should be noted that the hydrogen bonds created by the hydroxyl groups are all shorter than the conventional hydrogen bonds (>2.7 Å),[29] which may promote proton transfer and help to create radicals.[24] These results indicate that the intermolecular interaction is strengthened by the introduction of hydroxyl groups. In addition, the crystallized state of these compounds **PyTPA**, **PyTPA-OH** and **PyTPA-2OH** were further characterized by powder X-ray diffraction (PXRD), the PXRD analysis indicated that all compounds displayed sharp and intense diffraction pattern in crystallized (Figure S13).

### 2.3. Density function theory calculations

Density functional theory (DFT) calculations were performed to investigate the molecular geometry and the molecular frontier orbitals using the B3LYP-D3BJ at 6-31G (d,p) basis set. The optimized structures of the three molecules are presented in **Figure S15**. The methoxy TPAs splay out from the pyrene core in a star shape. These molecules exhibit a similar lowest unoccupied molecular orbital (LUMO) distribution. The LUMO is mainly localized on the central pyrene core, which helps to block the electron transportation. In the **PyTPA** molecule, the highest occupied molecular orbital (HOMO) spreads out all over the molecule. However, due to the presence of the steric effect of the hydroxyl groups at the 2- or 2,7-positions, a re-distribution of the HOMO is detected. The HOMOs of **PyTPA-OH** and **PyTPA-2OH** are mainly distributed at the central pyrene core and one diagonal pair of the TPA arms. It suggests the existence of intramolecular charge transfer (ICT) character,[30] which is beneficial to inducing charge separation. The calculated LUMO and HOMO energy levels are listed in **Table 1**. All these molecules possess suitable LUMO and HOMO values for obtaining energy level alignment in PSCs. The incorporation of the hydroxyl groups at the pyrene core slightly enlarges the band gap of the molecules, which is in agreement with our previous reports.[25]

### 2.4. The electrochemical properties and optical response

The electrochemical properties of these compounds were characterized in dichloromethane solution (~10 μM) through cyclic voltammetry (C-V). As shown in **Figure 3A**, the oxidation potentials for **PyTPA-OH** and **PyTPA-2OH** are 0.90 V and 0.86 V, respectively. These values are slightly higher than that of **PyTPA** (0.78 V), which indicates the enhanced oxidation ability due to the presence of the hydroxyl groups. All the materials show a clear quasi-reversible oxidation process with onset oxidation potentials ($E_{\mathrm{onset}}$) at 0.57 V, 0.60 V and 0.54 V for **PyTPA**, **PyTPA-OH** and **PyTPA-2OH**, respectively. The HOMO and LUMO levels were estimated using the empirical equations $E_{\mathrm{HOMO}} = -(E_{\mathrm{onset}} + 4.40)$ and $E_{\mathrm{LUMO}} = E_{\mathrm{HOMO}} + E_{\mathrm{g}}$, where $E_{\mathrm{g}}$ is the energy band gap determined through the onset of the optical absorption. All the results are displayed in **Table 1**. The calculated values for the HOMO and LUMO levels are not equal to the electrochemical data, and the main reasonis that the theoretical calculations are preformed in the gas phase and exclude intermolecular interactions. Meanwhile, the cyclic voltammogram experiments were carried out in solution; here the intermolecular interactions between the pyrene-based molecules, and between the pyrene-based molecules and the solvent molecules are complicated. These differences cause the electronic to be distribution different.

The optical absorption spectra of these pyrene core-based triphenylamines were characterized in THF solution at ~10 μM (**Figure 3B**). These materials exhibit strong absorption in the wavelength range from 250 to 350 nm, which is assigned to the $\pi$-$\pi^*$ transition. Attributed to the enhanced intermolecular interaction, the maximum value of the molar absorption coefficients ($\varepsilon$) is increased from 67000 $M^{-1}$ $cm^{-1}$ (**PyTPA**) to 90300 $M^{-1}$ $cm^{-1}$ (**PyTPA -2OH**). In the lower energy region (~350-500 nm) of the absorption spectrum, a sub-absorption is observed, which is related to the ICT transition.[28] As discussed in the previous section, the steric effect from the hydroxyl group(s) enlarges the torsion angle between the methoxy TPAs and the pyrene core. It leads to a HOMO redistribution, which plays a vital role in affecting the ICT process. With the increasing number of hydroxyl groups, a blue-shift of the ICT band is observed from 425 nm in the case of **PyTPA** to 399 nm in the case of **PyTPA-2OH**.

Photoluminescence (PL) characterization was conducted to investigate the excitation properties, as shown in **Figure 3B** and **3C**. All the materials emit green fluorescence in THF solution, with a maximum emission at 502 nm for **PyTPA**, 507 nm for **PyTPA-OH** and 507 nm for **PyTPA-2OH**. The fluorescence quantum yields ($\Phi_{\mathrm{f}}$) of these compounds are 0.70-0.79 in solution. This suggests that the presence of the hydroxyl groups has little impact on the emission behaviour of these materials in solution. A red-shifted emission is observed in the solid state of these compounds with a reduced $\Phi_{\mathrm{f}}$ (0.32-0.42), as listed in **Table 1**. Compared with the emission in solution, the PL of solid **PyTPA** peaks at 543 nm, which presents a large red-shift value of 41 nm. Attributed to the steric effect of hydroxyl groups, a much smaller red-shift value is detected in the solid state of **PyTPA-OH** (15 nm) and **PyTPA-2OH** (5 nm). These pyrene-core based triphenylamines are bipolar molecules with an electron donating-accepting structure. The methoxy TPA unit works as the electron donor, and the pyrene core serves as the acceptor. Therefore, all the materials exhibit a strong solvent polarity dependent fluorescence with a large red-shift ~120 nm, which results in a tuneable colour changing from blue to orange (**Figures S14-S19**). In addition, the three compounds exhibit dual emission in high polar solvent of acetonitrile (ACN), N,N-dimethylformamide (DMF) and dimethylsulfoxide (DMSO) solution with the dominated emission peak at ~581 nm nm and shoulder peaks at ~ 414 nm (Table S2). This is assigned to the charge transfer emission of these pyrene-based molecules and the emission of the pyrene parent, respectively.[31] The main reason contributed to that the triphenylamines-decorate pyrenes show better solubility in polar solvents, and the triphenylamine unit acts a rotator in solution, resulting in these compounds exhibit dual emission. This phenomenon is commonly observed in pyrene-based aggregation-induced emission.[16c] **The** fluorescent lifetimes were extracted from the time-resolved PL (TRPL) spectra, as displayed in **Figure 3D** and **Table 1**. All compounds exhibit a similar fluorescence lifetime (3.20-4.29 ns) in THF solution (**Figure S22**). **PyTPA** possesses the shortest lifetime with a value of 3.20 ns in solution and 1.73 ns in the solid state. The fluorescent lifetime of **PyTPA-OH** is 3.92 ns in solution and 3.16 ns in the solid state. In **PyTPA-2OH**, these values change to 4.29 ns and 3.10 ns, respectively. This suggests that the introduction of the hydroxyl groups contributes to a longer lifetime, also, the presence of the hydroxy groups on the pyrene core promote charge transfer and reduce the non-radiative recombination.

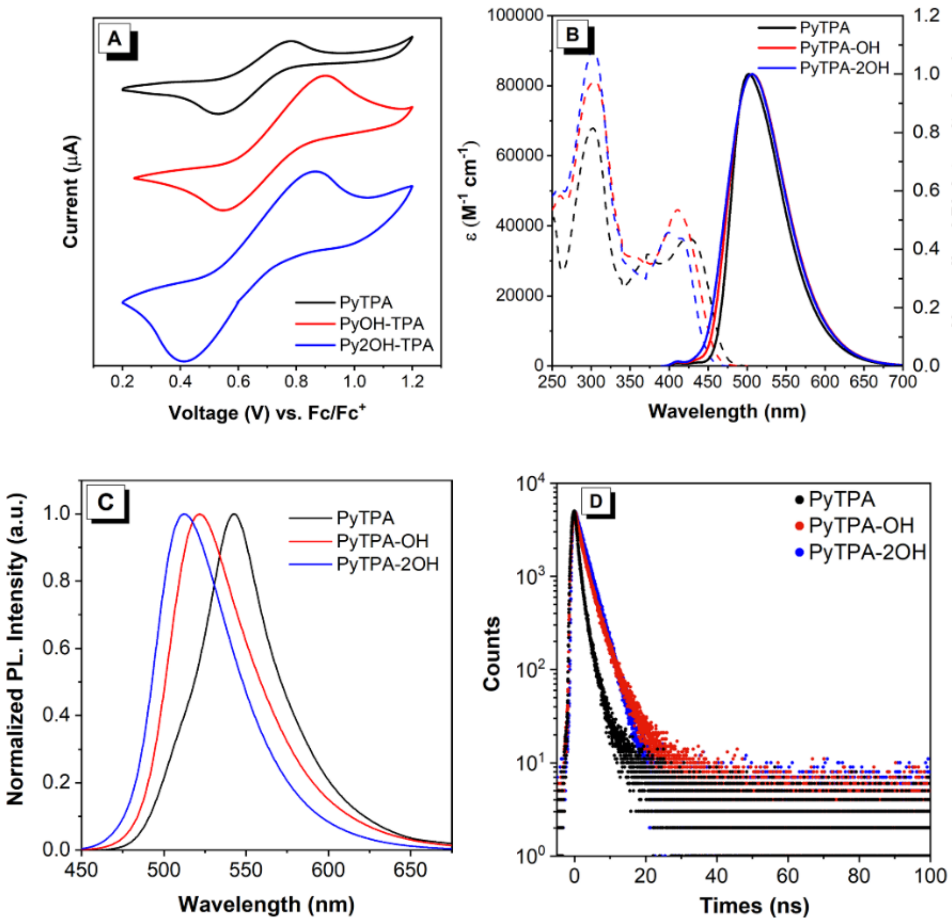

**Figure 3.** (A) Cyclic voltammograms of **PyTPA**, **PyTPA-OH** and **PyTPA-2OH** in dichloromethane at a scan rate of 100 mVs$^{-1}$; (B) UV-vis absorption and emission spectra in THF solution (~10$^{-5}$ M); (C) normalized steady-state PL spectra and (D) the decay curves of **PyTPA**, **PyTPA-OH** and **PyTPA-2OH** in the solid state.

**Table 1.** Summary of the electrochemical and optical properties of **PyTPA**, **PyTPA-OH** and **PyTPA-2OH**.

| HTMs | $\lambda_{max}^{abs}$ [nm] soln$^{a)}$/solid$^{b)}$ | $\lambda_{max}^{PL}$ [nm] soln$^{a)}$/solid$^{b)}$ | $\Phi_f$ sonl$^{a)}$/solid$^{c)}$ | $\tau$ [ns] soln$^{a)}$/ solid$^{b)}$ | $E_{LUMO}$ [eV] DFT$^{c)}$/Exp$^{d)}$ | $E_{HOMO}$ [eV] DFT$^{c)}$/Exp$^{e)}$ | $E_g$ [eV] DFT$^{c)}$/Opt$^{f)}$ | $T_d$$^{g)}$ [ºC] |
|---|---|---|---|---|---|---|---|---|
| **PyTPA** | 424 / 392 | 500 / 543 | 0.70 / 0.32 | 3.20 / 1.73 | -1.40 / -2.34 | -4.29 / -4.97 | 2.89 / 2.63 | 451 |
| **PyTPA-OH** | 411 / 408 | 507 / 522 | 0.74 / 0.36 | 3.92 / 3.16 | -1.39 / -2.27 | -4.33 / -5.00 | 2.94 / 2.73 | 445 |
| **PyTPA-2OH** | 399 / 396 | 507 / 512 | 0.79 / 0.42 | 4.29 / 3.10 | -1.33 / -2.19 | -4.32 / -4.94 | 2.99 / 2.75 | 452 |
| **Spiro-OMeTAD** | 388 / 393 | 502 / 532 | 0.68 / 0.29 | 3.18 / 2.48 | -1.45 / -2.36 | -4.27 / -4.91 | 2.82 / 2.55 | 458 |

[a] Measured in THF solution at room temperature; [b] Measured in solid at room temperature; [c] D3BJ/B3LYP at 6-31G (d,p) basis set calculations; [d] $E_{LUMO} = E_{HOMO} + E_g$; [e] Determined by C-V using ferrocene as the reference calculated by the empirical formula $E_{HOMO} = -(E_{ox}^{onset} + 4.40)$; [f] Extracted from optical absorption; [g] $T_d$ was obtained from the thermogravimetric analysis.

### 2.5. Behaviour under irradiation, EPR measurements and conductivity tests

These triphenylamines are designed for HTMs of PSCs, which always work under light irradiation. Herein, a light treatment of one sun irradiation (AM 1.5G, 100 Mw cm$^{-2}$) is conducted by exposing these samples to air. All the samples exhibit an original colour of yellow in the solid state. After irradiation, the colour of the **PyTPA-2OH** solid changes to black, while the colour of **PyTPA** and **PyTPA-OH** stays unchanged. The UV-vis-NIR spectroscopy of these compounds in the solid state was performed. Consistent with their unchanged colour, the light irradiation shows little impact on the absorption of **PyTPA** and **PyTPA-OH** (**Figure 4A** and **Figure S26**). The unirradiated **PyTPA-2OH** solid shows a main absorption with a peak at 472 nm and an absorption shoulder at ~570 nm. Its optical performance, especially in the long wavelength range (> 700 nm), is significantly improved by the irradiation (**Figure 4C**). A new absorption peak is observed at 861 nm, which can be also detected in the irradiated **PyTPA-OH** (~864 nm). This peak in the irradiated **PyTPA-OH** and **PyTPA-2OH** may be attributed to the formation of cation radicals by the hydroxyl groups and TPA units.[32]

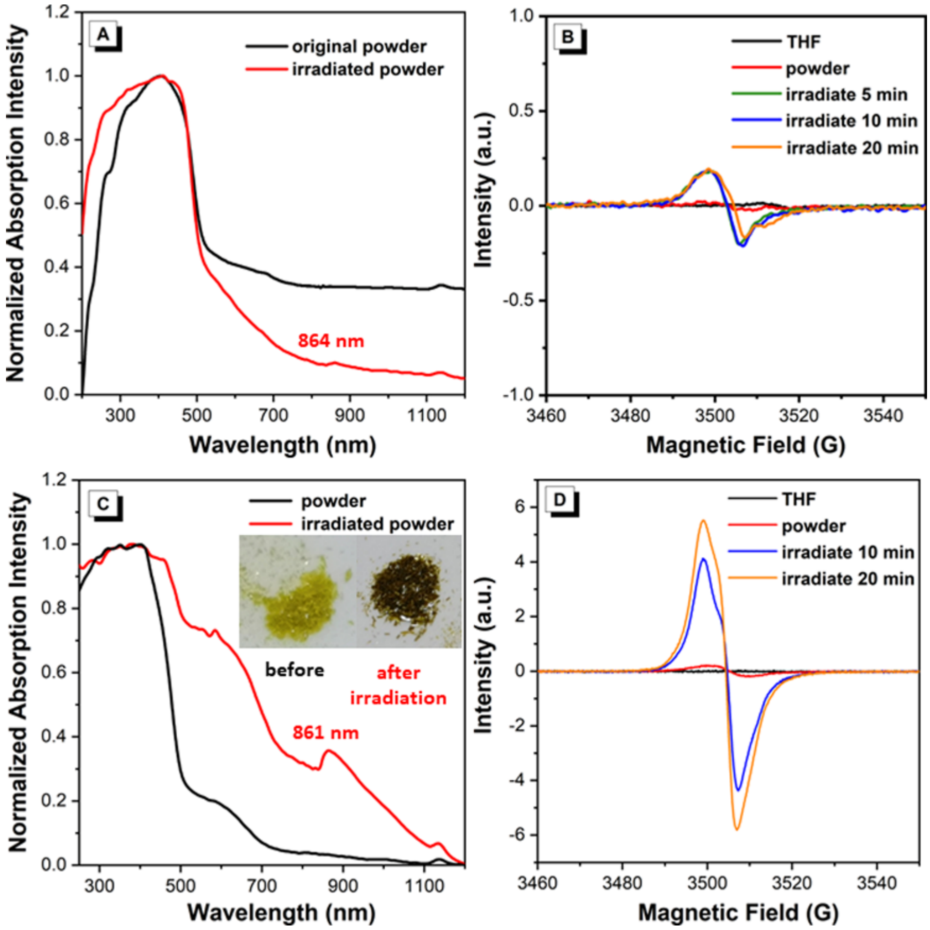

**Figure 4.** The NIR-UV-vis absorption of (A) **PyTPA-OH** and (C) **PyTPA-2OH**. The EPR spectra of (B) **PyTPA-OH** and (D) **PyTPA-2OH** in THF solution, and EPR spectra of (B) **PyTPA-OH** and (D) **PyTPA-2OH** powder before and after irradiation. The insert images are the powder of **PyTPA-2OH** before and after UV irradiation.

To explore the presence of radicals, the electron paramagnetic resonance (EPR) spectra were recorded (**Figure 4B**, **4D** and **Figure S27)**. All compounds in THF solution present extremely weak EPR signals. It suggests that the radicals are hard to generate in the solution. A faint EPR signal can be detected in the **PyTPA** powder before and after irradiation, indicating small amounts of radicals (**Figure S27).** Before irradiation, the **PyTPA-OH** powder shows a similar EPR signal with **PyTPA**, with a g-value of ~2.005 (**Table S4**). With the assistance of light irradiation (10 min), a clear EPR signal is observed with an intensity of 0.20. It suggests that the presence of the hydroxy group promotes the generation of radicals. However, extending the irradiation time is not able to enhance this signal. After 20 min irradiation, its intensity remains unchanged (**Figure 4B**). As show in Table S4, the g value of the pyrene-based HTMs is in range from 2.004-2.005 both in solution and in the solid state, indicating that the formed radical belongs to the TPA radical cation type.[33] With two hydroxy groups on the pyrene core, the non-irradiated **PyTPA-2OH** has already exhibited an EPR signal with a g-value of 2.005 and an intensity of 0.22 (**Figure 4D**). This signal is significantly enhanced by the irradiation. A strong EPR signal with an intensity of 4.37 is detected after 10 min of irradiation; it further increases to 5.82 with a 20 min irradiation. Thus, **PyTPA-2OH** shows a much stronger ability to generate radicals, compared with **PyTPA** and **PyTPA-OH**. These EPR results demonstrate the formation of radicals in **PyTPA-OH** and **PyTPA-2OH** under the irradiation of light, and that the introduction of hydroxyl groups allows these HTMs to generate radicals during the operation of PSCs. According to the previous analysis, the incorporation of hydroxyl groups will enhance the proton transfer through the shortened C-O bond and strengthened hydrogen bond, which promotes the formation of radicals. This increased radical density will lead to an improved film conductivity.[34]

The conductivity of these HTMs was studied by fabricating the HTM-only devices, with a device architecture of FTO/HTM/Ag. The direct current conductivity ($\sigma_0$) can be extracted by $J = \sigma_0 \cdot d^{-1} V$ (**Figure 5B**), where the d is the thickness of the sample.[35] The surface morphologies of the new HTMs deposited onto perovskite films were measured by atomic force microscope (AFM). As shown in Figure S28, by use of **PyTPA-OH** and **PyTPA-2OH**, the RMS value changes from 51.3 nm (perovskite layer: pristine) to 27.8 nm (**PyTPA-OH**), and 18.9 nm (**PyTPA-2OH**), respectively, this main reason is that the presence of two hydroxyl groups in the pyrene core can strength the intermolecular interactions between the PyTPA-2OH molecules, as well as between the PyTPA-2OH molecules and the surface of the PSK which prefer to form a smoother surface in on the surface of PSK via self-assemble in CB solution. On the other hand, the FT-IR spectra (Figure S29) indicate that the absorption bands of -OH group of **PyTPA-OH** and **PyTPA-2OH** are located at 3517 cm$^{-1}$ and 3410 cm$^{-1}$, which is shifted to 3512 cm$^{-1}$ and 3415 cm$^{-1}$ respectively, when these compounds are mixed with PbI. These results indicate that the HTM was interacted with the interfaces of underlayer perovskite weakly. Thus, the conductivity of the control HTM spiro-OMeTAD is 6.42×10$^{-4}$ S cm$^{-1}$, which is consistent with the previous reports.[6] [36] The **PyTPA** film exhibits a conductivity with a value of 6.78×10$^{-4}$ S cm$^{-1}$. This is slightly higher than that of spiro-OMeTAD, indicating its excellent charge transfer ability. On the other hand, considering the differences in the molecular structures of the pyrene core and Spiro-OMETAD, the former possesses a large-π-conjugated planar structure,[16] which is beneficial to improving the electronic and hole mobility of **PyTPA**. In contrast, the latter exhibits a topologic structure and two fluorene units separated by a sp$^3$ carbon, and the molecular conformation is unfavourable for charge transition.[37] Attributed to the increased radicals, the conductivity of **PyTPA-OH** jumps to 8.84×10$^{-4}$ S cm$^{-1}$. This value further increases to 9.42×10$^{-4}$ S cm$^{-1}$ in the film of **PyTPA-2OH**, which is ~39% higher than that of **PyTPA** and ~47% higher than that of spiro-OMeTAD. This suggests that the connection of the hydroxyl groups at the pyrene core greatly promotes the carrier transportation of HTMs, which is desired for charge extraction. An enhanced photovoltaic performance can be achieved by applying **PyTPA-2OH** as the HTM.

### 2.6. Device performance and stability tests

To explore the potential of these pyrene-based triphenylamines in photovoltaic applications, PSCs were fabricated using the n-i-p device architecture of FTO/$SnO_2$/$FAPbI_3$/HTMs/Ag. **PyTPA**, **PyTPA-OH** and **PyTPA-2OH** were applied as the HTMs, and the traditional HTM spiro-OMeTAD was selected as the control sample. At least 10 devices were fabricated for each condition. Both the DFT simulations and the experimental results illustrate that these pyrene-based HTMs are able to form a cascade energy alignment in the PSC (**Figure 5A**). The light intensity-dependent short circuit ($J_{SC}$) and open circuit voltage ($V_{OC}$) of the PSCs were measured to investigate the charge recombination behaviour influenced by these HTMs (**Figure S30** and **Figure 5C**). Both the exponential factor ($\alpha$) and the $n$ value are extracted.[38] All these PSCs exhibit a similar $\alpha$ value within the range from 0.991 to 0.997, which are all close to one. This demonstrates that all the devices possess excellent charge collection ability under short circuit conditions. The $n$ value can be used to evaluate the trap-assisted (Shockley-Read-Hall) recombination; a smaller $n$ value indicates less recombination. It has been demonstrated that improving the conductivity of the HTM promotes hole extraction and reduces the charge recombination.[39] The incorporation of hydroxyl groups contributes to an increased radical density and conductivity, which reduces the $n$ value. The extracted $n$ values of the spiro-

OMeTAD and the **PyTPA** based devices are 1.27 and 1.24, respectively. By increasing the number of hydroxyl groups at the pyrene core, the *n* value is decreased to 1.16 in the **PyTPA-OH** based device and to 1.03 in the **PyTPA-2OH** based device. This indicates an enhanced hole extraction ability in the **PyTPA-OH** and **PyTPA-2OH** based devices, which significantly suppresses the charge recombination. These results are consistent with the TRPL testing results (Figure 3D and Figure S22). Furthermore, an overall enhancement in the external quantum efficiency (EQE) spectra and the corresponding integrated current was observed in the PSCs with **PyTPA-OH** or **PyTPA-2OH** as the HTM. As shown in **Figure 5D**, the onset wavelength in the EQE spectrum is 768 nm, and the enhanced EQE in the range from 400 to 760 nm may be ascribed to the improvement of absorption efficiency and limited defects.[40] On the other hand, the EQE drop at around 400 nm is coincident with the absorption of the corresponding compounds. [41] The current density-voltage (*J*-*V*) curves and the photovoltaic parameters of these devices are presented in **Figure 5E** and **Table 2**. The **PyTPA** HTM exhibits a device performance with an average PCE of 21.41% with a $J_{SC}$ of 23.61 mA cm$^{-2}$ and a fill factor (FF) of 77.52%. Its PCE is slightly higher than that of the control device using spiro-OMeTAD (20.92%), indicating that **PyTPA** is a promising candidate as the HTM for PSCs.

**Table 2.** Photovoltaic performance of the devices with **PyTPA**, **PyTPA-OH** and **PyTPA-2OH** as the HTMs.[a]

| HTMs | $J_{SC}$ [mA cm$^{-2}$] | $V_{OC}$ [V] | FF [%] | PCE$^{avg}$ [%] | PCE$^{best}$ [%] |
|---|---|---|---|---|---|
| **PyTPA** | 23.61±0.07 | 1.17±0.003 | 77.52±0.07 | 21.41±0.08 | 21.49 |
| **PyTPA-OH** | 24.07±0.05 | 1.18±0.002 | 79.07±0.05 | 22.46±0.06 | 22.52 |
| **PyTPA-2OH** | 24.71±0.04 | 1.18±0.001 | 80.41±0.04 | 23.44±0.06 | 23.50 |
| **Spiro-OMeTAD** | 23.05±0.07 | 1.17±0.002 | 77.58±0.06 | 20.92±0.08 | 21.00 |

[a] The 30 PSC devices used to calculate the average photovoltaics parameters in Table 2.

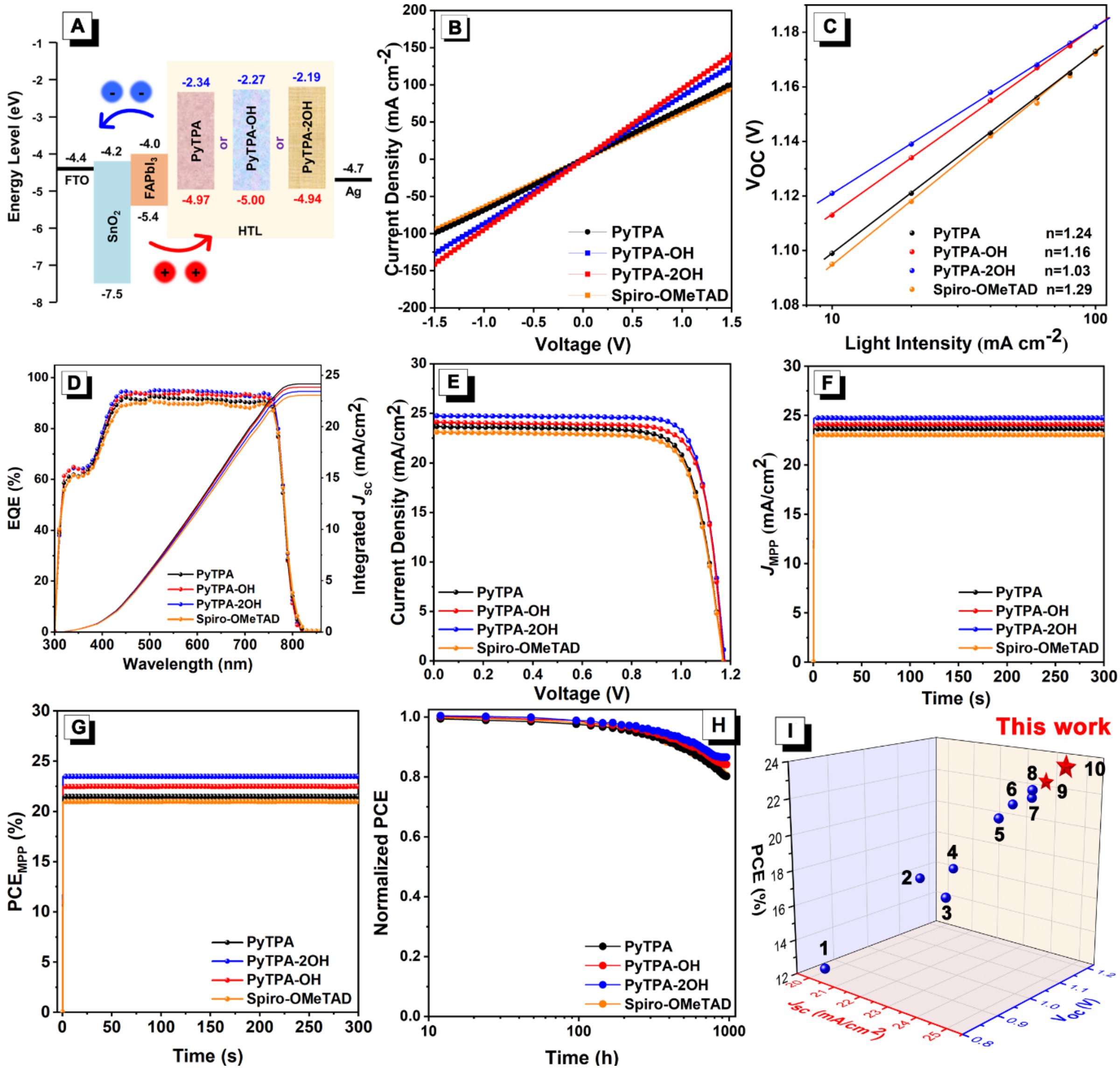

**Figure 5.** (A) Schematic energy-level diagram of the corresponding materials in the PSC; (B) Direct current conductivity measurement for **PyTPA**, **PyTPA-OH**, **PyTPA-2OH** and **Spiro-OMeTAD**; (C) Light intensity dependent-$V_{OC}$ curves; (D) EQE spectra with the corresponding integrated $J_{sc}$; (E) $J$-$V$ curves; (F) steady-state output current; (G) steady-state PCEs at the maximum power point; (H) stability test of the PSCs using **PyTPA**, **PyTPA-OH**, **PyTPA-2OH** and **Spiro-OMeTAD** as the HTM; (I) Comparison of the $V_{OC}$, $J_{SC}$ and PCE in the reported PSCs using pyrene-core based HTMs.[17] [18] [19] [42] The details of these pyrene-based HTMs are presented in **Scheme S2** and **Table S5**.

As discussed in the previous section, the hydroxy groups on the pyrene core contribute to a strong intermolecular interaction and a high density of radicals, which is beneficial for the hole transferring properties. Thus, both the $J_{SC}$ and FF of the PSCs are gradually improved with the increased number of hydroxy groups at the pyrene core. The $J_{SC}$ increases to 24.07 mA cm-

$^{2}$ in the case of **PyTPA-OH** and to 24.71 mA cm$^{-2}$ in the case of **PyTPA-2OH**, which is consistent with the EQE measurements. Meanwhile, the FF increases to 79.07% for the **PyTPA-OH** based device and to 80.41% for the **PyTPA-2OH** based device. As a result, the device with the **PyTPA-OH** HTM shows an average PCE of 22.46%. The best performance is obtained by applying **PyTPA-2OH** as the HTM. The PCE of the **PyTPA-2OH** based device shows an average PCE of 23.44% with a champion efficiency of 23.50%. It is the highest efficiency among the reported PSCs using a pyrene-core based HTM (**Figure 5I**). The steady-state output of the PSC at the maximum power point is measured by applying the corresponding voltage bias for more than 300 s. **Figure 5F** and **5G** show the time-dependent output current and PCE, respectively. In the spiro-OMeTAD, **PyTPA**, **PyTPA-OH** and **PyTPA-2OH** based devices, the stabilized current densities are 23.06 mA cm$^{-2}$, 23.66 mA cm$^{-2}$, 24.11 mA cm$^{-2}$ and 24.74 mA cm$^{-2}$, respectively. The corresponding stabilized PCEs are 20.99%, 21.48%, 22.49% and 23.49%, respectively. **Figure 5H** shows the stability of these PSCs. All the samples were store inside a glove box without encapsulation. All the devices exhibit a similar stability, which maintains 95% of the initial PCS after ~300 h and 85% after ~840 h. Benefited by the high decomposition temperature, these three pyrene-based HTMs ensure good stability. The reduction of the device performance is mostly attributed to the degradation of the FAPbI$_3$ layer.[43] In addition, the PSC device stability was further measured at 85$^{o}$C for 500 h under air. As shown in Figure S30, the pyrene-based devices maintained a relative high PCE value of 47% for **PyTPA**, 65% for **PyTPA-OH,** 75% for **PyTPA-2OH** compared to their initial value, respectively. For spiro-OMeTAD, the normalized PCE just maintained 32% over 312 h. On the other hand, the water contact angles on films of **PyTPA-OH** and **PyTPA-2OH** were measured with value of presented in Figure **S?**, Both compounds showed high hydrophobic properties with the average contact angles of 88.35$^{o}$ for **PyTPA-OH,** and 91.45$^{o}$ for **PyTPA-2OH,** respectively. The later shows higher hydrophobicity maybe the strengthen intermolecular interaction via the H-bond interaction, which is also beneficial to smooth the surface. This result is also consisting with the AFM results. With the number of -OH group increasing, the pyrene-based HTMs materials on the surface of the perovskite play a signficant role to boost the device stability. The enhanced device stability is mainly attributed to the presence of dopant-free HTM without post-oxidation, which provides a new direction for understanding the advantages of the pyrene-based molecular systems for perovskite solar cells applications.[44] These results demonstrate the great potential of these three pyrene-core based HTMs in obtaining efficient PSC.

## 3. Conclusions

In summary, three pyrene-core based triphenylamines with different numbers of hydroxy groups have been designed and synthesized through a Pd-catalyzed Suzuki-cross coupling reaction with high yield. All these materials have been shown to be a better HTM than the traditional HTM spiro-OMeTAD. The star-shaped molecule geometry of these molecules allows a tenon and mortise like intermolecular stacking structure. The presence of hydroxy groups introduces a steric effect into the molecule, which creates a large torsion angle between the methoxy TPA arms and the pyrene core. It leads to the redistribution of the HOMO and contributes to an ICT character. The intermolecular interaction is enhanced through the strong hydrogen bonding of the hydroxy groups, which promotes the generation of radicals. Therefore, a strong radical signal is detected in the solid **PyTPA-2OH** after the irradiation of a visible light. The strong intermolecular stacking and the high radical density endows **PyTPA-2OH** with an excellent hole transferring ability, which results in an improved conductivity and suppressed recombination. As a result, the best photovoltaic performance is achieved with an average PCE of 23.44% ($PCE_{max}$=23.50%) by applying **PyTPA-2OH** as the HTM, which is significantly higher than the control sipro-OMeTAD based device (20.92%). This research offers a new molecular design strategy for the HTM by the combination of pyrene core, methoxy TPAs and hydroxy groups.

## 4. Experimental Section

### 4.1 Materials

Unless otherwise stated, all reagents used were purchased from commercial sources and were used as received. Specpure grade solvents were used for spectroscopic measurements. The chemical intermediates 1,3,6,8-tetrabromopyrene, 2,7-dihydroxy-1,3,6,8-tetrabromopyrene (**1a**) and 2-hydroxy-1,3,6,8-tetrabromopyrene (**1b**) were synthesized following the reported procedures.[25]

### 4.2 The fabricated PSC devices

The device was fabricated with the configuration of FTO/$SnO_2$/Perovskite Layer/HTM Layer/Ag. The FTO glass was ultrasonically cleaned with distilled water containing detergent, dichloromethane, THF, and IPA in that sequence. Then, the FTO was treated by oxygen plasma for 5 min. The colloid of $SnO_2$ was dispersed into deionized water with the volume ratio of 1:4. $SnO_2$ solution (~100 μL) was spin-coated onto the FTO substrate with the speed of ~4000 rpm, and annealed in air for 30 min based on the temperature of ~150°C. The FTO with a $SnO_2$ layer was moved into a glove box with an argon atmosphere. The 1.65 M $PbI_2$ precursor solution was prepared by dissolving $PbI_2$ in a mixed solvent of DMF and DMSO with a volume ratio of 9:1.

The $PbI_2$ solution (85 μL) was spin-coated onto the FTO with a $SnO_2$ layer at the speed of ~1500 rpm, and then annealed at 65°C for 1 min. Subsequently, 85 μL of the mixed organic solution (mass ratio of FAI: MACl: MABr = 90 mg: 9 mg: 9 mg was dissolved in 1 mL IPA) was spin-coated onto the $PbI_2$ layer at the speed of ~2000 rpm. Then, they were transferred to air (RH = 40±5%) and annealed at ~150°C for 20 min. The PEAI was dissolved in IPA to obtain a solution of 1.25 mg $mL^{-1}$, and 80 μL of the solution was spin-coated on the perovskite layer at 4000 rpm. Then 960 mg spiro-OMeTAD or 1109 mg PyTPA, 16.8 μL Li-TFSI (520 mg $mL^{-1}$ solution dissolved in acetonitrile), 27.6 μL Co (III) FK209 TFSI (300 mg $mL^{-1}$ solution dissolved in acetonitrile) and 27.6 μL tetra-tert-butylpyridine were dissolved in CB together to prepare the HTL precursor solution. The HTL precursor solution was spin-coated onto the perovskite layer to form the HTL. For the pyrene derivatives of **PyTPA-OH** and **PyTPA-2OH**, the concentration of ~0.78 M was prepared in CB for the HTL without any additives. The thickness of the HTLs based on **PyTPA-OH** and **PyTPA-2OH** was measured by surface profilometer, and the thickness is 38.3 nm for **PyTPA-OH** and 38.8 nm for **PyTPA-2OH**, respectively. The HTL solution was spin-coated onto the PEAI layer (~4000 rpm). In the end, 100 nm of Ag was deposited on the HTL by using vacuum thermal evaporation.

### 4.3. Characterization

$^{1}H$ and $^{13}C$ NMR spectra (400 MHz) were recorded on a Bruker AV 400M spectrometer using chloroform-*d* solvent and tetramethylsilane as internal reference. *J*-values are given in Hz. High-resolution mass spectra (HRMS) were recorded on a LC/MS/MS, which consisted of a HPLC system (Ultimate 3000 RSLC, Thermo Scientific, USA) and a Q Exactive Orbitrap mass spectrometer. UV-vis absorption spectra and PL spectra were recorded on a Shimadzu UV-2600 and the Hitachi F-4700 spectrofluorometer. The PL quantum yields were measured using an integrating sphere using an Edinburgh FLS 980 instrument. The fluorescence lifetime was recorded on an Edinburgh FLS 980 instrument and measured using a time-correlated single-photon counting method. The prompt and delayed transient PL decay profiles were performed using a picosecond pulsed diode laser (EPL-375) and a variable pulse length diode laser (VPL-375) as the excitation sources, respectively. Thermogravimetric analysis was carried on a Mettler Toledo TGA/DSC3+ under dry nitrogen at a heating rate of 10 $^{o}C$/min. The quantum chemistry calculations were performed on the Gaussian 09 (B3LYP-D3BJ/6-31g(d,p) basis set) software package. C-V was performed with a standard three-electrode system, using glassy carbon electrode, Ag/AgCl and Pt Wire served as working electrode, the reference and counter electrodes, respectively. The measurements were collected in 0.10 M tetrabutylammonium perchlorate using ferrocenium/ferrocene as reference in THF with a scanning rate of 100 mV $s^{-}$

$^1$ at room temperature. EPR spectra were performed on a Bruker EMXplus-10/12 spectrometer. The *J*-*V* curves were obtained using a Keithley 2400 SourceMeter with a xenon-based solar simulator under AM 1.5G, 100 mW cm$^{-2}$ illumination, with a scanning rate of 10 mV s$^{-1}$ and an effective area of 0.06 cm$^2$. The EQE data of the PSCs were obtained in the direct-current mode using a calibrated spectrometer system (Enlitech QE-R). The conductivity was measured with the structure of ITO/HTM/Ag, and the *J*-*V* curves were obtained using a Keithley 2400 SourceMeter.

### 4.4. X-ray Crystallography

The X-ray crystallographic data for the compounds was collected on a Bruker APEX 2 CCD diffractometer with graphite monochromated Mo Kα radiation ($\lambda$ = 0.71073 Å) in the ω scan mode.[45] The structures were solved by charge flipping or direct methods algorithms and refined by full-matrix least-squares methods on $F^2$.[46] All esds (except the esd in the dihedral angle between two l.s. planes) were estimated using the full covariance matrix. The cell esds were considered individually in the estimation of esds in distances, angles and torsion angles. Correlations between esds in cell parameters were only used when they were defined by crystal symmetry. An approximate (isotropic) treatment of cell esds was used for estimating esds involving l.s. planes. The final cell constants were determined through global refinement of the xyz centroids of the reflections harvested from the entire data set. Structure solution and refinements were carried out using the SHELXTL-PLUS software package. Data (excluding structure factors) on the structures reported here have been deposited with the Cambridge Crystallographic Data Centre. CCDC 2280381 (**PyTPA**), 2280383 (**PyTPA-OH**) and 2280382(**PyTPA-2OH**), contains the supplementary crystallographic data for this paper. These data could be obtained free of charge from The Cambridge Crystallographic Data Centre via www.ccdc.cam.ac.uk/data_request/cif.

### 4.5 Materials Synthesis

#### *4.5.1 Synthesis of 1,3,6,8-tetrakis(4-(bis(4-methoxyphenyl)amino)phenyl)pyrene (PyTPA)*

1,3,6,8-tetrabromopyrene (207 mg, 0.4 mmol, 1.0 eq.), 4-(bis(4-methoxyphenyl)amino)phenyl boronic acid (830 mg, 2.4 mmol, 6.0 eq.) and $K_2CO_3$ (550 mg, 4 mmol, 10 eq.) was added into a mixture of toluene/ EtOH/ $H_2O$ (10 mL/ 2 mL/ 2 mL) under a nitrogen atmosphere. After stirring for 10 min, $Pd(PPh_3)_4$ (93 mg, 0.08 mmol, 0.2 eq.) was added. The mixture was vigorously stirred at 90°C for 24 h. After cooling to room temperature, the reaction mixture was quenched by water and extracted with $CH_2Cl_2$ three time. The combined organic layer was washed with brine, dried over $MgSO_4$ and evaporated. The crude product was purified by chromatography using $V_{hexane}/V_{CH2Cl2}$= 2:1, and then purified further by recrystallization from the mixture of $CH_2Cl_2$ and hexane to afford **PyTPA** as a yellow powder (460 mg, 81%). $^1$H NMR (400 MHz, $CDCl_3$, δ): 8.26 (s, 4H), 8.00 (s, 2H), 7.48 (d, *J* = 8.5 Hz, 8H), 7.17 (d, *J* = 8.8 Hz, 16H), 7.09 (d, *J* = 8.4 Hz, 8H), 6.88 (d, *J* = 9.0 Hz, 16H), 3.83 (s, 24H); $^{13}$C NMR (100 MHz, $CDCl_3$, δ): 155.9, 147.9, 141.0, 136.9, 133.2, 131.3, 129.4, 127.9, 126.7, 126.4, 125.1, 120.4, 114.8, 55.5. This data is corresponds with our previous report. [27]

### *4.5.2 Synthesis of 2-hydroxy-1,3,6,8-tetrakis(4-(bis(4-methoxyphenyl)amino)phenyl)pyrene (PyTPA-OH)*

The synthesis route of **PyTPA-OH** was similar to **PyTPA**, 1,3,6,8-tetrabromo-2-hydroxypyrene (192 mg, 0.4 mmol, 1.0 eq.), 4-(bis(4-methoxyphenyl)amino)phenyl boronic acid (740 mg, 2.2 mmol, 6.0 eq.) and $K_2CO_3$ (500 mg, 3.6 mmol, 10 eq.) was added into a mixture of toluene/ EtOH/ $H_2O$ (10 mL/ 2 mL/ 2 mL) under a nitrogen atmosphere. After stirring for 10 min, $Pd(PPh_3)_4$ (83 mg, 0.07 mmol, 0.2 eq.) was added. The mixture was vigorously stirred at 90°C for 24 h. After cooling to room temperature, the reaction mixture was quenched by water and extracted with $CH_2Cl_2$ three time. The combined organic layer was washed with brine, dried over $MgSO_4$ and evaporated. The crude product was purified by chromatography using $V_{hexane}/V_{CH2Cl2}$= 3:2, then purified further by recrystallization from $CH_2Cl_2$/ hexane to afford **PyTPA-OH** as a green powder (360 mg, 70%). $^1$H NMR (400 MHz, $CDCl_3$, δ): 8.21 (d, *J* = 9.6 Hz, 2H), 7.92 (s, 1H), 7.87 (d, *J* = 9.5 Hz, 2H), 7.46 (d, *J* = 8.5 Hz, 4H), 7.37 (d, *J* = 8.5 Hz, 4H), 7.17 (d, *J* = 9.4 Hz, 16H), 7.12 (d, *J* = 8.5 Hz, 4H), 7.08 (d, *J* = 8.5 Hz, 4H), 6.88 (d, *J* = 9.0, 3.0 Hz, 16H), 5.65 (s, 1H), 3.82 (s, 24H). $^{13}$C NMR (100 MHz, $CDCl_3$, δ): 156.1, 155.9, 148.6, 148.5, 147.9, 141.0, 140.8, 137.4, 133.2, 132.0, 130.5, 128.4, 126.9, 126.8, 126.7, 126.6, 125.8, 125.7, 124.7, 123.1, 120.8, 120.3, 120.2, 114.8, 114.7, 55.5. HRMS (FTMS+pAPCI) *m*/*z*: $[M + H]^+$ calcd for $C_{96}H_{78}N_4O_9$, 1432.587; found, 1432.5841.

### *4.5.3 Synthesis of 2,7-dihydroxy-1,3,6,8-tetrakis(4-(bis(4-methoxyphenyl)amino)phenyl)pyrene (PyTPA-2OH)*

The synthesis route of **PyTPA-2OH** was similar to **PyTPA-OH** and **PyTPA**. 1,3,6,8-tetrabromo-2,7-dihydroxypyrene (220 mg, 0.4 mmol, 1.0 eq.), 4-(bis(4-methoxyphenyl)amino)phenyl boronic acid (830 mg, 2.4 mmol, 6.0 eq.) and $K_2CO_3$ (552 mg, 4 mmol, 10 eq.) was added into a mixture of toluene/ EtOH/ $H_2O$ (10 mL/2 mL/2 mL) under a nitrogen atmosphere. After stirring for 10 min, $Pd(PPh_3)_4$ (93 mg, 0.08 mmol, 0.2 eq.) was added. The mixture was vigorously stirred at 90°C for 24 h. After cooling to room temperature, the reaction mixture was quenched by water and extracted with $CH_2Cl_2$ three time. The combined organic layer was washed with brine, dried over $MgSO_4$ and evaporated. The crude product was purified by chromatography using $V_{hexane}/V_{CH2Cl2}$= 1:1, and then purified further by recrystallization from $CH_2Cl_2$/ hexane to afford **4TPA-27-OH** as green crystals (410 mg, yield 71%). $^1$H NMR (400 MHz, $CDCl_3$, δ): 7.84 (s, 4H), 7.35 (d, *J* = 8.5 Hz, 8H), 7.18 (d, *J* = 8.8 Hz, 16H), 7.11 (d, *J* = 8.4 Hz, 8H), 6.88 (d, *J* = 8.9 Hz, 16H), 5.59 (s, 2H), 3.82 (s, 24H). $^{13}$C NMR (100 MHz, $CDCl_3$, δ): 156.1, 148.5, 147.8, 140.8, 132.0, 129.3, 127.2, 126.9, 125.4, 123.6, 120.3, 120.4, 114.8, 55.5. HRMS (FTMS+pAPCI) *m*/*z*: $[M + H]^+$ calcd for $C_{96}H_{78}N_4O_{10}$, 1447.5791; found, 1447.5749.

**Supporting Information**

Supporting Information is available from the Wiley Online Library or from the author.

**Acknowledgements**

This work was supported by the National Natural Science Foundation of China (21975054, 22375043), Guangdong Basic and Applied Basic Research Foundation (2020A1515110992), Industry -University Project of Fujian Provincial Department of Science and Technology (2023H6037), the Open Fund of Guangdong Provincial Key Laboratory of Luminescence from Molecular Aggregates, Guangzhou 510640, China (South China University of Technology) (2019B030301003), Science and Technology Planning Project of Hunan Province (2018TP1017). CR thanks the University of Hull for funding and XF thanks Dr. Jianyu Zhang (HKUST) for the DFT and TD-DFT calculations.

**Competing interest**

The authors declare they have no competing interests.

**Additional information**

All data are available in the paper and/or the Supplementary Materials.

Received: ((will be filled in by the editorial staff))
Revised: ((will be filled in by the editorial staff))
Published online: ((will be filled in by the editorial staff))

References

[1] J. Y. Kim, J. W. Lee, H. S. Jung, H. Shin, N. G. Park, *Chem. Rev.* **2020**, *120*, 7867-7918.

[2] a) N. J. Jeon, H. Na, E. H. Jung, T. Y. Yang, Y. G. Lee, G. Kim, H. W. Shin, S. I. Seok, J.

Lee, J. Seo, *Nat. Energy* **2018**, *3*, 682-689; b) H. Li, W. Zhang, *Chem. Rev.* **2020**, *120*, 9835-9950; c) Q. Jiang, J. H. Tong, Y. M. Xian, R. A. Kerner, S. P. Dunfield, C. X. Xiao, R. A. Scheidt, D. Kuciauskas, X. M. Wang, M. P. Hautzinger, R. Tirawat, M. C. Beard, D. P. Fenning, J. J. Berry, B. W. Larson, Y. F. Yan, K. Zhu, *Nature* **2022**, *611*, 278-283; d)Y. Zhao, F. Ma, Z. Qu, S. Yu, T. Shen, H. X. Deng, X. Chu, X. Peng, Y. Yuan, X. Zhang, J. You, *Science* **2022**, *377*, 531-534; e) X. Zhu, R. Lin, H. Gu, H. Hu, Z. Liu, G. Xing, Y. Wu, X. Ouyang, *Energy Environ. Mater.***2023**, *6*, e12426.

[3] a) K. Akihiro, T. Kenjiro, S. Yasuo, M. Tsutomu, *J. Am. Chem. Soc.* **2009**, *131*, 6050-6051; b) J. Park, J. Kim, H. S. Yun, M. J. Paik, E. Noh, H. J. Mun, M. G. Kim, T. J. Shin, S. l. Seok, *Nature* **2023**, *616*, 724-730; c) F. Z. Qiu, M. H. Li, J. J. Qi, Y. Jiang, J. S. Hu, *Aggregate* **2021**, *2*, 66-83; d) H. Lin, M. Yang, X. Ru, G. Wang, S. Yin, F. Peng, C. Hong, M. Qu, J. Lu, L. Fang, C. Han, P. Procel, O. Isabella, P. Gao, Z. Li, X. Xu, *Nat. Energy*, **2023**, *8*, 789-299.

[4] a) X. Yin, Z. Song, Z. Li, W. Tang, *Energy Environ. Sci.* **2020**, *13*, 4057-4086; b) P. Murugan, T. Hu, X. Hu, Y. Chen, *J. Mater. Chem.* **2022**, *10*, 5044-5081.

[5] a) H. Min, D. Y. Lee, J. Kim, G. Kim, K. S. Lee, J. Kim, M. J. Paik, Y. K. Kim, K. S. Kim, M. G. Kim, T. J. Shin, S. I. Seok, *Nature* **2021**, *598*, 444-450; b) M. Kim, J. Jeong, H. Lu, T. K. Lee, F. T. Eickemeyer, Y. Liu, I. W. Choi, S. J. Choi, Y. Jo, H. B. Kim, S. I. Mo, Y. K. Kim, H. Lee, N. G. An, S. Cho, W. R. Tress, S. M. Zakeeruddin, A. Hagfeldt, J. Y. Kim, M. Gratzel, D. S. Kim, *Science* **2022**, *375*, 302-306.

[6] Z. Li, J. Tinkham, P. Schulz, M. Yang, D. H. Kim, J. Berry, A. Sellinger, K. Zhu, *Adv. Energy. Mater.* **2017**, *7*, 1601451.

[7] a) U. B. Cappel, T. Daeneke, U. Bach, *Nano Lett.* **2012**, *12*, 4925-4931; b) J. Kong, Y. Shin, J. A. Rohr, H. Wang, J. Meng, Y. Wu, A. Katzenberg, G. Kim, D. Y. Kim, T. D. Li, E. Chau, F. Antonio, T. Siboonruang, S. Kwon, K. Lee, J. R. Kim, M. A. Modestino, H. Wang, A. D. Taylor, *Nature* **2021**, *594*, 51-56; c) F. Ma, Y. Zhao, Z. Qu, S. Yu, Z. Chu, Z. Xiong, J. Zhou, Z. Wei, X. Zhang, J. You, *Solar RRL* **2023**, *7*, 2300042.

[8] Z. Hawash, L. K. Ono, Y. Qi, *Adv. Mater. Interfaces* **2016**, *3*, 1600117.

[9] a) Z Hawash, L. K. Ono, S. R. Raga, M. V. Lee, Y. Qi, *Chem. Mater.* **2015**, *27*, 562-569; b) C. C. Boyd, R. Cheacharoen, T. Leijtens, M. D. McGehee, *Chem. Rev.* **2019**, *119*, 3418-3451; c) G. Ren, W. Han, Y. Deng, W. Wu, Z. Li, J. Guo, H. Bao, C. Liu, W. Guo, *J. Mater. Chem. A* **2021**, *9*, 4589-4625.

[10] a) X. Sun, X. Yu, Z. Li, *ACS Appl. Energy Mater.* **2020**, *3*, 10282-10302; b) P. Yan, D. Yang, H. Wang, S. Yang, Z. Ge, *Energy. Environ. Sci.* **2022**, *15*, 3630-3669.

[11] W. Ling, F. Liu, Q Li, Z. Li, *J. Mater. Chem. A* **2021**, *9*, 18148-18163.

[12] A. M. Onteria, I. Zimmermann, I. G. Benito, P. Gratia, C. R. Carmona, S. Aghazada, M. Graetzel, *Angew. Chem. Int. Ed.* **2016**, 55, 6270-6274.

[13] a) R. Azmi, S. Y. Nam, S. Sinaga, Z. A. Akbar, C. L. Lee, S. C. Yoon, I. H. Jung, S. Y. Jang *Nano Energy* **2018**, *44*, 191-198; b) R. Xue, M. Zhang, D. Luo, W. Chen, R. Zhu, Y. M. Yang, Y. Li, Y. Li, *Sci. China Chem.* **2020**, *63*, 987-996; c) X. Zhang, X. Liu, R. Ghadari, M. Li, Z. Zhou, Y. Ding, M. Cai, S. Dai, *ACS Appl. Mater. Interfaces* **2021**, *13*, 12322-12330.

[14] Z. Wang, S. Yan, Z. Yang, Y. Zou, J. Chen, C. Xu, P. Mao, S. Ding, J. Chen, X. Zong, T. Qin, M. Liang, *Chem. Eng. J.* **2022**, *450*, 138189.

[15] H. Guo, H. Zhang, C. Shen, D. Zhang, S. Liu, Y. Wu, W. H. Zhu, *Angew. Chem. Int. Ed.* **2021**, *60*, 2674-2679.

[16] a) T. M. Figueira-Duarte, K. Müllen, *Chem. Rev.* **2011**, *111*, 7260-7314; b) X. Feng, J. Y. Hu, C. Redshaw, T. Yamato, *Chem. Asian J.* **2016**, *22*, 11898-11916 (2016); c) M. M. Islam, Z. Hu, Q. Wang, C. Redshaw, X. Feng. *Mater. Chem. Front.* **2019**, *3*, 762-781; d) X. Feng, X. Wang, C. Redshaw, B. Z. Tang, *Chem. Soc. Rev.* **2023**, *52*, 6715-6753.

[17] a) Z. Yao, F. Zhang, L. He, X. Bi, Y. Guo, Y. Guo, L. Wang, X. Wan, Y. Chen, L. Sun. *Angew. Chem. Int. Ed.* **2022**, *61*, e202201847; b) Y. Ou, A. Sun, H. Li, T. Wu, D. Zhang, P. Xu, R. Zhao, L. Zhu, R. Wang, B. Xu, Y. Hua, L. Ding, *Mater. Chem. Front.* **2021**, *5*, 876-884; c) J. Y. Shao,B. Yu, Y. D. Wang, Z. R. Lan, D. Li, Q. Meng, Y. W. Zhong, *ACS Appl. Energy Mater.* **2020**, *3*, 5058-5066; d) M. H. Li, T. G. Sun, J. Y. Shao,Y. D. Wang, J. S. Hu, Y. W. Zhong, *Nano Energy* **2021**, *79*, 105462.

[18] N. J. Jeon, J. Lee, J. H. Noh, M. K. Nazeeruddin, M. Grätzel, S. I. Seok, *J. Am. Chem. Soc.* **2013**, *135*, 19087-19090.

[19] Q. Q. Ge, J. Y. Shao, J. Ding, L. Y. Deng, W. K. Zhou, Y. X. Chen, J. Y. Ma,L. J. Wan, J. Yao, J. S. Hu, Y. W. Zhong, *Angew. Chem. Int. Ed.* **2018**, *57*, 10959-10965.

[20] a) Y. Zhang, B. Huang, M. Hu, B. Tan, F. Huang, Y. B. Cheng, A. N. Simonov, J. Lu, *J Mater. Chem. A* **2022**, *10*, 10604-10613; b) S. You, H. Zeng, Y. Liu, B. Han, M. Li, X. Zheng, R. Guo, L. Luo, Z. Li, C. Zhang, R. Liu, Y. Zhao, S. Zhang, Q. Peng,T. Wang, Q. Chen, F. T. Eickemeyer, B. Carlsen, S. M. Zakeeruddin, L. Mai, Y. Rong, M. Gratzel, X. Li, *Science* **2023**, *379*, 288-294.

[21] a) G. W. Kim, H. Choi, M. Kim, J. Lee, S. Y. Son, T. Park, *Adv Energy Mater.* **2020**, *10*, 1903403; b) A. Farokhi, H. Shahroosvand, G. D. Monache, M. Pilkington, M. K. Nazeeruddin, *Chem. Soc. Rev.* **2022**, *51*, 5974-6064.

[22] a) E. Moulin, J. J. Armao IV, N. Giuseppone, *Acc. Chem. Res.* **2019**, *52*, 975-983; b) A. J. Sindt, B. A. DeHaven, R. L. Goodlett, J. O. Hartel, P. J. Ayare, Y. Du, M. D. Smith, A. K. Mehta, A. M. Brugh, M. D. E. Forbes, C. R. Bowers, A. K. Vannucci, L. S. Shimizu, *J. Am. Chem. Soc.* **2020**, *142*, 502-511.

[23] Q. Xue, M. Liu, Z. Li, L. Yan, Z. Hu, J. Zhou, W. Li, X. F. Jiang, B. Xu, F. Huang, Y. Li, H. L. Yip, Y. Cao, *Adv. Funct. Mater.* **2018**, *28*, 1707444.

[24] Z. Li, Y. Wang, G. Baryshnikov, S. Shen, M. Zhang, Q. Zou, H. Agren, L. Zhu, *Nat. Commun.* **2021**, *12*, 908.

[25] a) X. Wang, J. Zhang, X. Mao, Y. Liu, R. Li, J. Bai, J. Zhang, C. Redshaw, X. Feng, *J. Org. Chem.* **2022**, *87*, 8503-8514; b) J. Voskuhl, M. Giese, *Aggregate* **2022**, *3*, e124.

[26] F. M. Rombach, S. A. Haque, T. J. Macdonald, *Energy Environ. Sci.* **2021**, *14*, 5161-5190.

[27] Y. Liu, Y. Wang, X. Song, X. Wang, H. Zhu, J. Zhang, J. Bai, C. Redshaw, X. L. Ni, X. Feng, D. Wang, B. B. Tang, *J. Mater. Chem. C* **2022**, *10*, 8783-8790.

[28] B. K. Sharma, A. M. Shaikh, N. Agarwal, R. M. Kamble, *RSC Adv.* **2016**, *6*, 17129-17137.

[29] T. Steiner, G. R. Desiraju, *Chem. Commun.* **1998**, 891-892.

[30] Ooyama, S. Inoue, T. Nagano, K. Kushimoto, J. Ohshita, I. Imae, K. Komaguchi, Y. Harima, *Angew. Chem. Int. Ed.* **2011**, *50*, 7429-7433.

[31] a) J. Wang, Q. Dang, Y. Gong, Q. Liao, G. Song, Q. Li, Z. Li, *CCS Chem.* **2021**, *3*, 274-286; b) X. Feng, C. Qi, H.-T. Feng, Z. Zhao, H. H. Y. Sung, I. D. Williams, R. T. K. Kwok, J. W. Y. Lam, A. Qin, B. Z. Tang. *Chem. Sci.*, **2018**, *9*, 5679–5687.

[32] X. Liu, Y. Zhao, Y. Ni, F. Shi, X. Guo, C. Li, *Energy Environ. Sci.* **2023**, *16*, 4065-4072.

[33] a) A. J. Sindt, B. A. DeHaven, D. F. McEachern, Jr, D. M. M. M. Dissanayake, M. D. Smith, A. K. Vannucci, L. S. Shimizu, *Chem. Sci.* **2019**, *10*, 2670-2677. b) A. R. Forrester, J. M. Hay and R. H. Thompson, Organic Chemistry of Stable Free Radicals, Academic Press, New York, 1968.

[34] T. Zhang, F. Wang, H. B. Kim, I. W. Choi, C. Wang, E. Cho, R. Konefal, Y. Puttisong, K. TERADO, L. Kobera, M. Chen, M. Y.ang, S. Bai, B. Yang, J. Suo, S. C. Yang, X. Liu, F. Fu, H. Yoshida, W. M. Chen, J. Brus, V. Coropceanu, A. Hagfeldt, J. L. Bredas, M. Fahlman, D. S. Kim, Z. Hu, F. Gao, *Science* **2022**, *377*, 495-501.

[35] J. Obrzut, K. A. Page, *Phys. Rev. B* **2009**, *80*, 195211.

[36] H. J. Snaith, M. Grätzel, *Appl. Phys. Lett.* **2006**, *89*, 262114.

[37] E. Fasani, M. Fagnoni, D. Dondi, A. Albini, *J. Org. Chem.* **2006**, *71*, 2037-2045

[38] a) L. J. A. Koster, V. D. Mihailetchi, R. Ramaker, P. W. M. Blom, *Appl. Phys. Lett.* **2005**, *86*, 123509; b) S. R. Cowan, A. Roy, A. J. Heeger, *Phys. Rev. B*, **2010**, *82*, 245207.

[39] Y. Yao, C. Cheng, C. Zhang, H. Hu, K. Wang, S. D. Wolf, *Adv. Mater.* **2022**, *34*, e2203794.

[40] X. Zhu, R. Lin, H. Gu, H. Hu, Z. Liu, G. Xing, Y. Wu, X. Ouyang, *Energy Environ. Sci.* **2022**, *6*, e12426.

[41] a) C. Y. Xu, W. Hu, G. Wang, L. Niu, A. M. Elseman, L. Liao, Y. Yao, G. Xu, L. Luo, D. Liu, G. Zhou, P. Li, Q. Song, *ACS Nano* **2020**, *14*, 196-203. b) Im, J. H.; Jang, I. H.; Pellet, N.; Gratzel, M.; Park, N. G., *Nat. Nanotechnol.* **2014**, **9**, 927-932.

[42] a) J. Qiu, H. Liu, X. Li, S. Wang, *Chem. Eng. J.* **2020**, *387*, 123965; b) H. Liu, Q. Chen, F. Wu, X. Liu, *J Phys. Chem. C* **2022**, *126*, 160-168.

[43] H. Liu, N. Li, Z. Chen, S. Tao, C. Li, L. Jiang, X. Niu, Q. Chen, F. Wang, Y. Zhang, Z. Huang, T. Song, H. Zhou, *Adv. Mater.* **2022**, *34*, e2204458.

[44] C. Liu, C. Igci, Y. Yang, O. A. Syzgantseva, M. A. Syzgantseva, K. Rakstys, H. Kanda, N. Shibayama, B. Ding, X. Zhang, V. Jankauskas, Y. Ding, S. Dai, P. J. Dyson, M. K. Nazeeruddin, *Angew. Chem. Int. Ed.* **2021**, *60*, 20489-20497.

[45] a) Saint, Sadabs, Bruker AXS Inc; Madison, Wisconsin, USA **2009**; b) SHELXTL Program Package, version 5.1, Bruker AXS, Inc: Madison, WI **1997**.

[46] G. M. Sheldrick, SHELXS97 and SHELXL97. Program for Crystal Structure Solution and Refinement; University of Göttingen, Göttingen **1997**.

## Table of Contents

# *In-situ* Photogenerated Radicals of Hydroxyl Substitued Pyrene-based Triphenylamines with Enhanced Transport and Free Doping/Post-oxidation for Efficient Perovskite Solar Cells

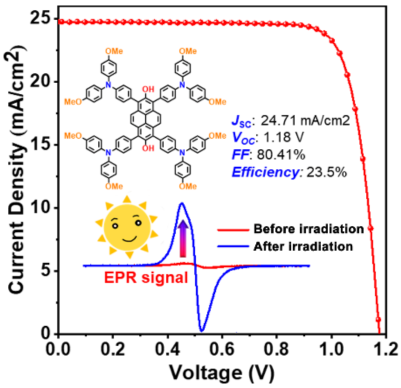

The pyrene-based HTMs exhibit excellent performance in PSCs with a short-circuit current density ($J_{SC}$)of 24.71 mA/cm$^2$, open-circuit voltage ($V_{oc}$) of 1.18 V, and a fill factor (*FF*) of 80.41%, with the highest PCE of 23.5%.an average PCE of 23.44 % (PCE$_{max}$ = 23.50%), which is the highest PCE reported to-date for PSCs with a pyrene-core based HTM.